GEOPHYSICAL RESEARCH LETTERS, VOL. 25, NO. 21, PAGES 3983-3986, NOVEMBER 1, 1998

Global scale decadal climate variability

Gerald A. Meehl, Julie M. Arblaster, Warren G. Strand Jr.,

National Center for Atmospheric Research Boulder, Colorado

Abstract. Analysis of observations and results from a global coupled climate model show that coherent decadal climate variability extends over the entire Pacific basin, is associated with processes in the Atlantic and Indian Ocean regions to contribute to global patterns of decadal climate variability, and encompasses regional decadal mechanisms noted in previous studies. Ocean heat content anomalies embedded in the gyre circulations of the Pacific, Atlantic and Indian Oceans are associated with global decadal timescale "El Niño-like" signals in atmosphere and ocean with consequent global energy balance variations. Large-scale tropical-midlatitude interactions act to replenish the ocean heat content anomalies. Maxima in decadal timescale globally averaged surface temperature occur in conjunction with periodic arrangements of SST anomalies, in association with the heat content anomalies embedded in the various ocean gyre circulations, in a global "El Niño-like" pattern that is highly correlated with such maxima. The decadal timescale in the model is approximately set by the circuit times of the ocean gyre circulations.

1. Introduction

To explain observed decadal timescale variability, previous studies have proposed regional mechanisms involving ocean heat content anomalies, ocean gyre circulations, and coupled feedbacks with the atmospheric circulation for the North Pacific, North Atlantic, and tropical Atlantic (see review by Latif, 1998 and references therein). So-called "El Niño-like" signals in the tropical Pacific on the decadal timescale have been noted in observations [Kang, 1996; Zhang et al., 1997] and coupled models [Knutson and Manabe, 1998].

At least part of the pattern of low frequency variability of the climate system, particularly the "El Niño-like" response associated with increasing CO_2 in the models, may be linked to low frequency variability in external forcing [e.g. Meehl and Washington, 1996; Haywood et al., 1997]. Consequently, it is important to understand the mechanisms that are producing the internally generated decadal variability to help sort out the climate change detection/attribution problem.

Paper number GRL-1998900088.
0094-8276/98/GRL-1998900088$05.00

Here we analyze 95 years from an integration of a global coupled ocean-atmosphere-sea ice climate model (R15 9L atmosphere, 1 degree by 1 degree 20L ocean, dynamic/thermodynamic sea ice; [Meehl and Washington, 1995; Washington and Meehl, 1996] along with near-global surface temperatures from 1900 to 1994 [Jones, 1988]. The purpose is to identify the mechanism that is generating global scale internally generated decadal variability (defined as periods of roughly 9-20 years) in the model, and to determine if we can infer from the model and the limited observations the mechanism in the real climate system.

2. Results

To separate the interannual from the decadal signals, we use an 8 year 73 point low pass Lanczos filter applied to the detrended monthly anomalies of SST from 95 years of surface air temperatures from the coupled model control case with constant CO_2 (Fig. 1a-d). Spectra of globally averaged surface temperature time series from the observations (not shown) and the model (Fig. 2a) show statistically significant spectral peaks in the El Niño period of around 4 years, and in the decadal period of around 13-14 years.

The high pass filtered time series are then formed by subtracting the low pass filtered data from the original time series. For an area in the Pacific from 15N to 15S, 157.5E to 82.5W, EOFs are calculated from the filtered data using the correlation matrix technique and the corresponding principle component time series (Fig. 1b,d) are then correlated with the filtered time series to form the patterns shown in Fig. 1a and c. Though the tropical Pacific is used as a base area here, as noted below there is a high correlation with low pass filtered globally averaged temperatures, and similar patterns are obtained using global surface temperatures [Meehl et al., 1997].

The model shows large positive correlations close to the equator for the high pass filtered data (Fig. 1c), while the low pass positive correlation values in the tropical Pacific (Fig. 1a) are spread in a wider off-equatorial range. Both high pass and low pass filtered data have opposite sign correlations in the northwest and southwest Pacific similar to the observations (not shown here, but refer to comparable plots in Zhang et al., 1997, Fig. 3; Knutson and Manabe, 1998, Fig. 4). This coupled model has some of the same systematic errors of others of its class [e.g. Meehl and Arblaster, 1998] in that the El Niño variability is about half of the

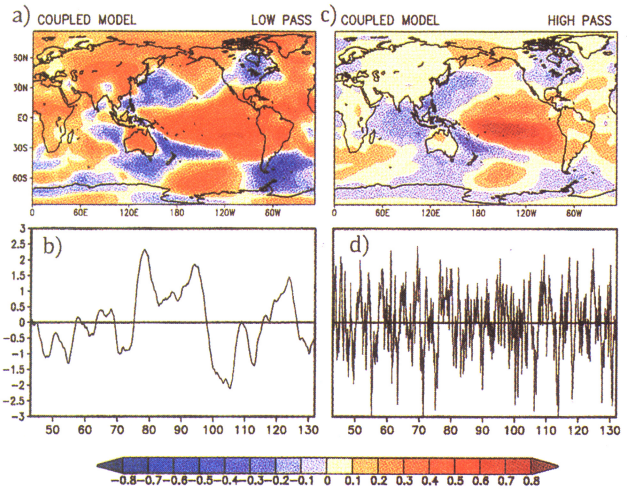

Figure 1. a) EOF1 from low pass filtered surface temperatures b) PC time series for low pass filtered EOF1; c) same as (a) except for high pass filtered data; d) same as (b) except for high pass filtered data.

observed, and the maximum model interannual Pacific equatorial variability is near the Dateline and somewhat south of the equator, with less high amplitude variability in the equatorial eastern Pacific.

The first EOF principal component (PC) time series of low pass filtered surface temperature, indicative of the time evolution of the dominant pattern of variability, is highly correlated with globally averaged surface temperature on the decadal timescale [+0.61 for the observations (not shown), and +0.89 for the model; note that this correlation pattern is associated with high amplitude temperature signals over the northern continents shown by regression analysis, Stouffer et al., 1994]. When global temperatures are warm on the decadal timescale, SSTs in the tropical Pacific are also warm in both observations and the model. Actual peak-to-peak amplitudes of SST anomalies on the decadal timescale reach about 1C – 1.5C locally in the model.

Vertically averaged temperature (VAT) over the upper 300 m of the ocean, a measure of heat content, is lag correlated with the low pass filtered EOF1 PC time series of surface temperature (Fig. 1b). Successive position of positive lag correlation values greater then +0.4 are shown at lag -8 and lag -4 years (Fig. 2b). An elaboration of this movement of heat content anomalies is illustrated for a full cycle for lag -10 years, lag 0 and lag +10 (Fig. 2c,d,e). As noted above, the EOF1 PC time series of low pass filtered surface temperature is highly correlated with globally averaged surface temperature, and we use the former to show the relationship between the global pattern of surface temperature and the upper ocean heat content.

The essence of the mechanism that is generating a considerable part of the internal decadal variability in the model can be seen as a global system of propagating heat content anomalies in all ocean basins (Fig. 2c-e) corresponding to the ocean gyre circulations (Fig. 2f). The largest amplitude lag correlations are in the range of ± 0.4–0.6 which are significant at the 5% level and explain up to 40% of the variance locally.

The advective timescale in the model subtropical gyres (taking a typical current speed at a depth of 87.5 m to be 0.04 m s^{-1}, and one full circuit around the gyre to be 2×10^7 m) is 15.9 years. Thus, the decadal timescale of global climate variability in the model is ap-

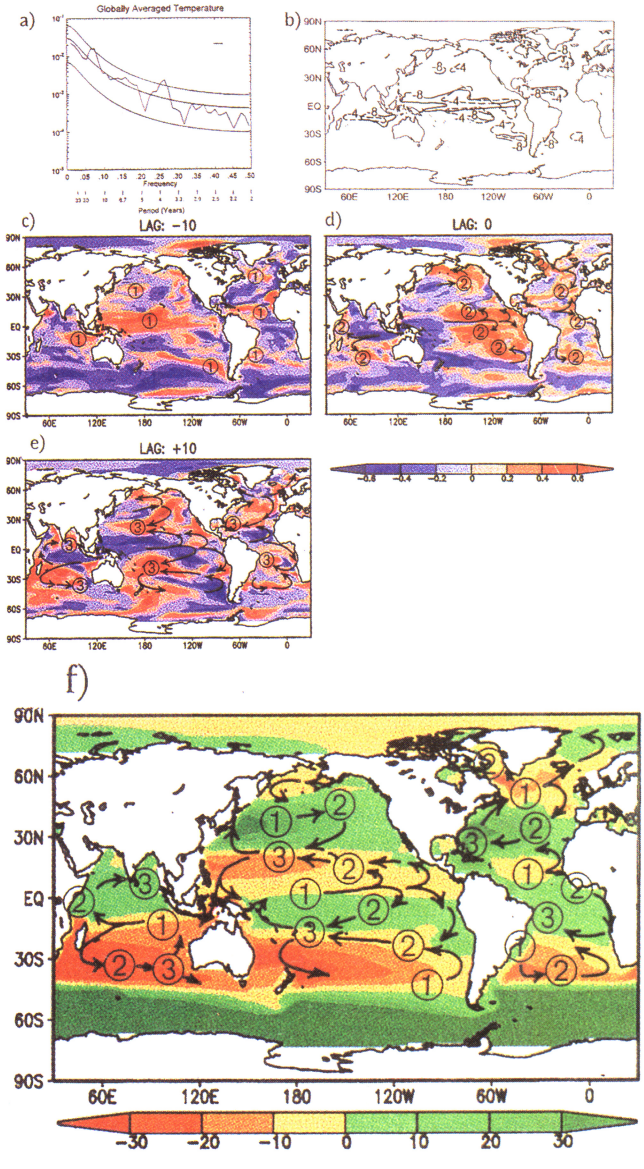

Figure 2. (a) Spectra of globally averaged surface temperature for the 95 years of model simulation. Peaks exceeding top line are significant at the 95% level. EOF1 PC time series of low pass filtered surface temperature from the model (Fig. 1b) lag correlated with vertically averaged ocean temperature (upper 300 m) (b) showing successive position of significant areas of positive lag correlation greater than +0.4 at lags -8 and -4, and total plots for (c) lag -10 years (d) lag 0, (e) lag+10; (f) approximate positions of maxima of positive lag correlations in panels c-e, with the numbers 1 through 3 representing lags -10 years, lag 0, and lag +10 years, respectively, superimposed on ocean mass transport streamfunction.

proximately set by the advective timescale of the ocean gyre circulations.

Coupled atmosphere-ocean-sea ice interactions in the model are illustrated by various indices lag correlated with globally averaged surface air temperature (Fig. 3; all time series have been low-pass filtered). For the Pacific (Fig. 3a), El Niño-like relationships on the decadal timescale are evident whereby a maximum of central equatorial Pacific precipitation is associated with a maximum in global temperature (as well as a maximum of SST in the tropical Pacific, Fig. 1a), and a minimum of South Asian monsoon precipitation. El Niño-like teleconnections to the midlatitudes, associated with the anomalous convective heating from the eastward shift of precipitation due to the warming of central and eastern tropical Pacific SSTs, intensify the troughs in the north and south Pacific (Fig. 3a). This has been noted to occur on the decadal timescale in the observations for the Aleutian Low [e.g. Trenberth and Hurrell, 1994] and the South Pacific trough [e.g. Karoly et al., 1996]. Ocean-atmosphere coupling in these areas provides a feedback mechanism for replenishment of the ocean heat content anomalies through the surface energy balance. That is, equatorward advection of cold air on the west side of the troughs in the north and south Pacific contributes to negative net heat flux (negative lag correlations for north Pacific net heat flux in Fig. 3a), which contributes to decreased SST and lower VAT (note negative SST (Fig. 1a) and negative heat content lag correlations (Fig. 2d) in those regions).

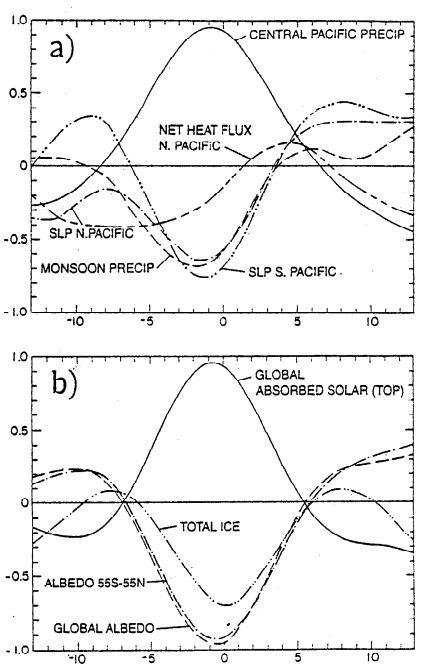

Figure 3. Low pass filtered annual mean indices from the coupled model lag correlated with annual mean globally averaged surface air temperature a) central Pacific precipitation (5N to 5S, 150E to 170W), Asian monsoon precipitation (land points only averaged in the area 5N to 40N, 60E to 100E), SLP in the North Pacific (30N to 50N, 160E to 180), net surface heat flux in the North Pacific (30N to 50N, 160E to 180), and SLP in the south Pacific (30S to 50S, 180 to 160W); b) same as (a) except for quantities affecting global energy balance.

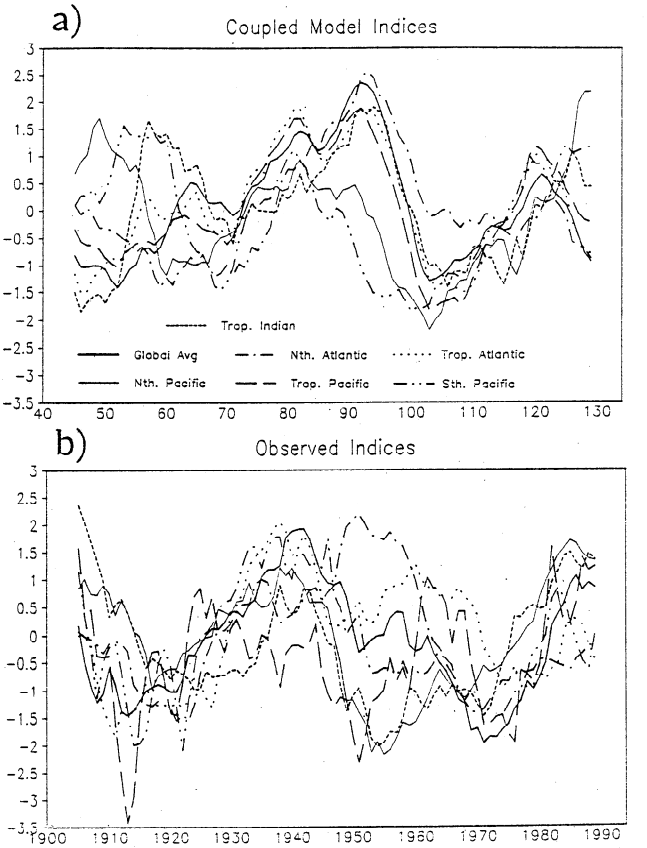

Figure 4. Area-averaged 11 year running mean SST indices N. Pacific (35N-45N, 150E-175E), S. Pacific (30S-40S, 180E-150W), Nino3.4 (5N-5S, 170W-120W), N. Atlantic (30N-45N, 50W-75W), Trop. Atlantic (Eq.-12N, 25W-50W), Indian (15S-30S, 60E-90E); a) coupled model, and b) observations.

As these El Niño-like responses on the decadal timescal affect global temperature, other feedbacks involving clouds and sea ice come into play and contribute to amplifying the oscillation associated with the VAT anomalies in Fig. 2. Greater convection in the central equatorial Pacific is associated with increased high cloud albedos [Meehl and Washington, 1995], but the suppressed convection over the Asian-Australian monsoon regions (Fig. 3a) produces less clouds and consequent decreased albedo there. This effect, coupled with decreases of sea ice as the temperatures warm, contributes to decreased planetary albedo and increased absorbed solar radiation in conjunction with a maximum of globally averaged temperature in the model (Fig. 3b).

Though the propagation of heat content anomalies in all ocean basins appear to be synchronized to produce these patterns in a lag correlation sense, a better assessment of the relationships between the basins is gained by forming time series area-averaged SST indices indicative of activity in the ocean gyre circulations. These index regions were chosen because of their high correlation between VAT and SST (all greater than +0.6 except for the tropical Atlantic) indicating areas of strong linkage between the upper ocean and atmosphere. Fig. 4 shows the normalized time series of these indices as 11 year running means (to further emphasize the low

Table 1: Correlations between low pass SST indices and global temperature; a positive value of "lag" means the maximum lag occurs after the maximum of global temperature. North and South Pacific indices multiplied by -1.

	Model			Observed		
Index	simultaneous	maximum	lag	simultaneous	maximum	lag
Nth. Atlantic	+0.69	+0.77	+3	+0.58	+0.80	+8
Nth. Pacific	+0.12	+0.28	–6	+0.40	+0.45	–3
Sth. Pacific	–0.12	+0.34	+9	+0.82	+0.82	0
Trop. Atlantic	+0.93	+0.93	0	+0.66	+0.74	+3
Trop. Indian	+0.69	+0.69	0	+0.25	+0.25	0
Trop. Pacific	+0.91	+0.92	+1	+0.39	+0.39	0

frequencies), along with similarly filtered globally averaged surface temperature for the model and observations (north and south Pacific indices multiplied by -1 to be consistent in sign; see Fig. 1a). All indices except north and south Pacific from the model and tropical Indian in the observations are significantly correlated at the 5% level with globally averaged temperature at zero lag Table 1. Some indices have higher correlations at non-zero lags indicating various other timescales are operating in the basins. The correlation of the average of the indices with global temperature is +0.75 for the observations and +0.85 for the model, but as seen from the lag correlations, not all indices follow each other or the globally averaged temperature at all times. For example, in the coupled model there is a peak in globally averaged temperature around year 92, but the north and south Pacific indices are dropping at that time (Fig. 4). However, the north and south Pacific indices join the others in contributing to the minimum of global temperature around year 105. Similarly in the observations, a drop of globally averaged temperature around 1950 is receiving influences from the tropical Pacific, north Pacific and tropical Indian indices, while the north Atlantic and tropical Atlantic indices are rising, even though those latter two indices have statistically significant lag 0 correlations overall with global temperature (Table 1). Thus, though there is a range of correlations between the indices and global temperature, large-scale coupled interactions (e.g. Fig. 3) contribute to the organization of these patterns such that the decadal timescale alignments are not purely coincidental. Contributions from different regions, even those with low overall correlation, occur periodically (Fig. 4). In combination with these coupled processes shown in Figs. 2-4, the decadal timescale of around 13-14 years in the model for global climate variability, then, is approximately set by the average circuit time of the ocean gyre circulations.

Acknowledgments. The authors thank Warren Washington, James Hurrell, John Weatherly, and Dennis Shea for helpful discussions and comments. A portion of this study was supported by the Office of Biological and Environmental Research, U.S. Department of Energy, as part of its Carbon Dioxide Research Program. The National Center for Atmospheric Research is sponsored by the National Science Foundation.

References

Haywood, J. M., R. J. Stouffer, R. T. Wetherald, S. Manabe, and V. Ramaswamy, Transient response of a coupled model to estimated changes in greenhouse gas and sulfate concentrations. *Geophys. Res. Lett.*, **24**, 1335–1338, 1997.

Jones, P. D., Hemispheric surface air temperature variations: Recent trends and an update to 1987. *J. Climate*, **1**, 654-660, 1988.

Kang, I.-S., Association of interannual and interdecadal variations of global-mean temperature with tropical Pacific SST appearing in a model and observations. *J. Climate*, **9**, 455–464, 1996.

Karoly, D. J., P. Hope, and P. D. Jones, Decadal variations of the Southern Hemisphere circulation.*Int. J. Climatol.*, **16**, 723–738, 1996.

Knutson, T., S. and Manabe, Model assessment of decadal variability and trends in the tropical Pacific Ocean. *J. Climate*, in press, 1998.

Latif, M., Dynamics of interdecadal variability in coupled ocean-atmosphere models. *J. Climate*, **11**, 602–624, 1998.

Meehl, G. A., and J. Arblaster, The Asian-Australian monsoon and El Nino–Southern Oscillation in the NCAR Climate System Model. *J. Climate*, **11**, 1357–1387, 1998.

Meehl, G. A., and W. M. Washington, Cloud albedo feedback and the super greenhouse effect in a global coupled GCM. *Climate Dyn.*, **11**, 399–411, 1995.

Meehl, G. A., and W. M. Washington, El Niño-like climate change in a model with increased atmospheric CO_2 concentrations. *Nature*, **382**, 56–60, 1996.

Meehl, G. A., J. M. Arblaster, and W. G. Strand, Mechanisms of decadal variability related to globally averaged surface temperature. In *Proceedings of the Twenty-Second Annual Climate Diagnostics and Prediction Workshop*, Berkeley, CA, 6-10 October, 1997, U.S. Department of Commerce, Washington, D.C., 100–103, 1997.

Stouffer, R. J., S. Manabe, and K. Ya. Vinnikov, Model assessment of the role of natural variability in recent global warming. *Nature*, **367**, 634–636, 1994.

Trenberth, K. E. and J. W. Hurrell, Decadal atmosphere-ocean variations in the Pacific. *Climate Dyn.*, **9**, 303–319, 1994.

Washington, W. M. and G. A. Meehl, High latitude climate change in a global coupled ocean-atmosphere-sea ice model with increased atmospheric CO_2. *J. Geophys. Res.*, **101**, 12,795–12,801, 1996.

Zhang, Y., J. M. Wallace, and D. S. Battisti, Enso-like decade-to-century scale variability: 1900-93. *J. Climate*, **10**, 1004–1020, 1997.

G. A. Meehl, J. M. Arblaster and W. G. Strand Jr., National Center for Atmospheric Research, P.O. Box 3000, Boulder, CO 80307-3000. (email: meehl@ncar.ucar.edu)
color figs. at http://www.cgd.ucar.edu/ccr/Decadal

(Received May 12, 1998; revised September 2, 1998; accepted September 17, 1998.)